NIH Public Access
Author Manuscript
J Mol Biol. Author manuscript; available in PMC 2014 August 09.

Published in final edited form as:
J Mol Biol. 2013 August 9; 425(15): 2752–2764. doi:10.1016/j.jmb.2013.04.030.

PH-TRIGGERED CONFORMATIONAL SWITCHING OF THE DIPHTHERIA TOXIN T-DOMAIN: THE ROLES OF N-TERMINAL HISTIDINES

Igor V. Kurnikov[1], **Alexander Kyrychenko**[2,§], **Jose Christian Flores-Canales**[1], **Mykola V. Rodnin**[2], **Nikolay Simakov**[3], **Mauricio Vargas-Uribe**[2], **Yevgen O. Posokhov**[2,§], **Maria Kurnikova**[1,*], and **Alexey S. Ladokhin**[2,*,†]

[1]Chemistry Department, Carnegie Mellon University, Pittsburgh, PA 15213

[2]Department of Biochemistry and Molecular Biology, University of Kansas Medical Center, Kansas City, KS 66160-7421

[3]Center for Computational Research, SUNY, Buffalo, NY 14203

Abstract

pH-Induced conformational switching is essential for functioning of diphtheria toxin, which undergoes a membrane insertion/translocation transition triggered by endosomal acidification as a key step of cellular entry. In order to establish the sequence of molecular rearrangements and side chain protonation accompanying the formation of the membrane-competent state of the toxin's translocation (T) domain, we have developed and applied an integrated approach that combines multiple techniques of computational chemistry (e.g., long, μsec-range, all-atom molecular dynamics simulations; continuum electrostatics calculations; and thermodynamic integration) with several experimental techniques of fluorescence spectroscopy. Thermodynamic integration calculations indicate that protonation of H257 causes the greatest destabilization of the native structure (6.9 kcal/mole), which is consistent with our early mutagenesis results. Extensive equilibrium MD simulations with a combined length of over eight μsec demonstrate that histidine protonation, while not accompanied by the loss of structural compactness of the T-domain, nevertheless results in substantial molecular rearrangements characterized by the partial loss of secondary structure due to unfolding of helices TH1 and TH2, and the loss of close contact between the C- and N-terminal segments. The structural changes accompanying the formation of the membrane-competent state ensure an easier exposure of the internal hydrophobic hairpin formed by helices TH8 and TH9, in preparation for its subsequent transmembrane insertion.

Keywords

acid-induced conformational change; membrane protein insertion; histidine protonation; molecular dynamics; fluorescence; conformational switch

[†]This research was supported by NIH grant GM-069783

© 2013 Elsevier Ltd. All rights reserved.

[*]To whom correspondence should be addressed: aladokhin@kumc.edu or kurnikova@cmu.edu.
[§]Permanent address for A.K, and Y.O.P. is Institute for Chemistry, V. N. Karazin Kharkiv National University, 4 Svobody Sq., Kharkiv 61022, Ukraine

Publisher's Disclaimer: This is a PDF file of an unedited manuscript that has been accepted for publication. As a service to our customers we are providing this early version of the manuscript. The manuscript will undergo copyediting, typesetting, and review of the resulting proof before it is published in its final citable form. Please note that during the production process errors may be discovered which could affect the content, and all legal disclaimers that apply to the journal pertain.

NIH-PA Author Manuscript
NIH-PA Author Manuscript
NIH-PA Author Manuscript

NIH-PA Author Manuscript

NIH-PA Author Manuscript

NIH-PA Author Manuscript

Conformational switching, broadly defined as an alteration in the spatial organization of a macromolecule in response to environmental changes, binding of a ligand or proteolytic cleavage, is at the core of any cell function. The design of specific switches leading to changes between folded and disordered states or between distinct folds, as well as between different oligomeric states, is also an important topic in protein engineering [1]. pH-triggered switching, which utilizes the ability of the cell to regulate proton concentrations in different compartments, has been implicated in the entry of multiple bacterial toxins (e.g., diphtheria, botulinum, tetanus, and anthrax [2; 3; 4; 5; 6; 7]) and viruses [8; 9] sharing the endosomal pathway as well as in the regulation of apoptosis [10; 11; 12]. Here we utilize experimental approaches, an array of molecular modeling methods, and novel computational capabilities of ANTON, a specialized super-computer, designed to generate extra-long (μsec-range) molecular dynamics (MD) simulations [13; 14], to elucidate the molecular mechanism of conformational switching by protonation in diphtheria toxin translocation (T) domain.

The function of the T-domain is to translocate the catalytic domain across the lipid bilayer in response to acidification of the endosome [15], which requires a substantial refolding of the globular structure (see Fig. 1A for crystallographic structure [16]) and insertion into the membrane 17; 18; 19; 20 Previously we have demonstrated that the first step of this complex conformational transition of the T-domain, namely the formation of the membrane-competent state, occurs in solution at mildly acidic pH [20] and that histidine protonation is likely involved in various stages of conformational switching [21; 22; 23]. It remains unknown, however, what specific structural changes occurring in response to histidine protonation prepare the hydrophobic core of the T-domain for subsequent membrane insertion. To characterize molecular rearrangements and to explore the role of histidine protonation in conformational changes, we carried out multi-μsec molecular dynamics (MD) simulations of the T-domain in explicit solvent. Two MD simulations were performed, starting with the known structure of the T-domain in solution (Fig. 1A): one with all six native histidine residues in a standard (unprotonated) state (this corresponds to a membrane-incompetent state of the T-domain populated at neutral and high pH); and another with all histidines protonated (this corresponds to a membrane-competent state of a protein formed upon acidification). The simulations revealed a specific and subtle conformational transition, which prepares the protein for further interactions with the lipid bilayer. Several predictions based on MD simulations were validated experimentally using fluorescence spectroscopy. The role of individual histidines in T-domain conformational switching has been evaluated by all-atom Thermodynamic Integration (TI) simulation and by continuum electrostatics calculations, based on solving the Poisson-Boltzmann (PB) equation as pioneered by Honig and co-workers [24; 25], and implemented in the HARLEM molecular modeling package 26; 27

Results

Experimental evidence of pH-dependent formation of membrane-competent conformation

Formation of the membrane-competent form (W^+-state) of the T-domain is the first step along a complex pathway, leading from a soluble conformation with a known crystallographic structure (W-state) ultimately to membrane-inserted states, for which no high-resolution structural information is available. The W-to-W^+ conversion is the first pH-dependent conformational transition along this pathway and is normally identified in a membrane binding assay conducted under conditions of saturation with lipid vesicles [20]. We illustrate in Fig. 1B the application of three independent membrane binding methods to the T-domain's interaction with vesicles (raw data are shown in Supplementary Information Figs. S1A-C) based on: diffusion measurements by FCS (diamonds), association of donor-labeled T-domain and acceptor-labeled vesicles by FRET (circles) and changes in polarity of a specifically attached environment-sensitive bimane probe by increase in fluorescence

NIH-PA Author Manuscript

NIH-PA Author Manuscript

NIH-PA Author Manuscript

intensity (triangles). All datasets are adequately described by a single fitting curve with a pKa of 6.2 and Hill coefficient of about 2. Is it possible to correlate this pH-dependent binding with conformational changes in solution? This is not trivial, because in the absence of membranes under acidic conditions the T-domain aggregates avidly [28; 29], leading to poorly reproducible results, especially at pH<5.5. Nevertheless, when the tryptophan fluorescence intensity and ellipticity at 222 nm measured in solution are normalized in the pH range of 5.5÷8 (Fig. 1C), their relative changes correlate well with an accurately measured binding curve (solid line). This confirms that the W^+-state is not just a virtual thermodynamic state (e.g., similar to unfolded melittin on membrane interface [30]), or an unstable intermediate on the kinetic path from the W-state to a membrane-bound protein, but a relatively stable experimentally observable state of the protein with conformation different from that of the W-state. Next, we examine structural rearrangements along the W-to-W^+ transition via MD simulations employing protonation of all six histidine residues as a pH-dependent trigger.

Extended MD simulations of conformational change triggered by protonation of histidines

T-domain is composed of nine alpha helices (further termed TH1-TH9) [16] and has a globular structure in aqueous solution at neutral pH. Helices TH8 and TH9 constitute the hydrophobic core of the protein partially protected from water by the rest of the structure (Fig. 1A). At low pH the T-domain has been demonstrated to insert into lipid bilayer in a transmembrane conformation [17; 18; 19; 20]. However, little is known about specific structural changes initiated by His residue protonation. In order to shed light on how structural changes are initiated in solution upon protonation of the His residues, we performed molecular dynamics simulations of the T-domain in explicit aqueous solution mimicking both low-pH and high-pH conditions. To simulate the globular membrane incompetent W-state of the protein that occurs at neutral or basic pH, it was assumed that all protonatable residues of the protein were in their standard protonation states, including six histidines in neutral form. To simulate formation of a membrane-competent W^+-state, populated at mildly acidic pH [20], all six His residues of the T-domain were protonated. Protonation of all histidines provides the largest possible driving force for structure destabilization associated with lowered pH. Thus, we design a simulation with enhanced possibility of observing a structural transition on the MD simulation time-scale. Currently, there are no direct measurements of the protonation of the histidines in the T-domain, while indirect measurements give conflicting answers to the question whether histidines in the T-domain are protonated sequentially or cooperatively in solution or near the membrane interface [21;22; 23] . Therefore in our analysis we considered two separate questions: (1) what is the impact of His protonation on the protein structure and (2) what is the role of individual His residues in initiating and driving structural transition toward the W^+-state?. The former question is addressed in this section, while the latter one is deferred to the next (see the next section for a detailed analysis and discussion of individual pKas and their role in driving structural transition of the protein).

In the neutral pH simulation of approximately 2 μsec, the protein retained its globular structure in a natively folded state. The absence of significant structural changes during the entire simulation is evident from low values (about 1.9 Å) of the average root mean squared deviation (RMSD) of the Cα atoms in TH1–9 from their crystallographic positions (blue trace in Fig. 2A).

In stark contrast to the neutral pH simulation, large structural changes were observed in the protein during the 6 μs simulation at low pH. In Fig. 2A, the Cα RMSD plot shows an abrupt increase at 532 ns (dark yellow trace). This is primarily due to formation of a kink in helix TH1, initiated by rotation of backbone dihedral angles of K216 (see also Supplemental Information movie SI_movie_1_all.avi). This results in a decrease in α-helical content on

NIH-PA Author Manuscript

NIH-PA Author Manuscript

NIH-PA Author Manuscript

the C-terminus of TH1 followed by unfolding of its N-terminal. The subsequent partial refolding of TH1 is initiated in its N-terminus at 1037 ns. The resulting structure is stabilized by packing against TH9. Helix TH2 unwinds at 1414 ns followed by the C-terminal refolding of TH1 at 1482 ns (see also the description and the movie in Supplemental Information, SI_movie_2_TH1_TH2.avi). Thereafter, the Cα RMSD remains at a stable value, around 3.8 Å, over the last 2 μsec of the simulation. Note that the low value of RMSD prior to *ca.* 500 ns is similar to that for the neutral pH simulation. Therefore a conventional MD simulation (typically tens of nanoseconds in length for a system of this size) would have failed to detect the structural implications of histidine protonation. The dynamics of partial unfolding, subsequent refolding and further reorganization of the entire protein secondary structure is clearly seen in the plot of a fraction of α-helical content shown in Fig. 2B. Note that the observed conformational changes in the global structure also resulted in repositioning of the two histidines H223 and H257 with respect to each other. These residues, located in TH1 and TH5, respectively, are in close proximity to each other in the initial undisturbed structure, but move apart in the partially unfolded and refolded structures (see Supplemental Information, SI_movie_3_H223_H257.avi). This conformational transition also caused H257 to become exposed to the solvent, which is likely to provide the driving force for the observed refolding process (see section ***Thermodynamic integration and continuum electrostatics analysis of histidine protonation)*** As a consequence of the observed transition, the hydrophobic helices TH8 and TH9 become somewhat exposed to the solution, forming a membrane-competent state, a precursor state for the association with the membrane in the insertion process. The solvent accessible surface area (SASA) of hydrophobic side chains in helices TH8–9 increases along the low-pH T domain trajectory (red traces in Figs. 3A and 3B) relative to the average SASA of the same helices along the neutral-pH trajectory (shown as blue dashed lines in Figs. 3A and 3B).

Experimental validation of MD simulation results

We have used several spectroscopic techniques to validate various aspects of the MD-based conformational predictions. First, we examined the overall changes in secondary structure by measuring CD spectra (Fig. 1C and Supplemental Results Fig. S1C). At mildly acidic pH, the T-domain undergoes partial unfolding, and the resulting loss of ellipticity is consistent with that expected from unwinding of the TH1–2 segment (SI_movie_2_THl_TH2.avi). Second, we measured the intrinsic fluorescence from the two tryptophan residues (W206 and W281). While formation of the membrane-competent state is accompanied by a small decrease in intensity, the position of the maximum of emission remains constant in this pH range (from 8 to 5.5) and does not shift until a much lower pH is reached (Supplemental Results Fig. S1B). This is consistent with a lack of exposure of tryptophan residues to the aqueous phase predicted by the MD simulations. Third, the overall retention of the compact conformation during the formation of the membrane-competent state (SI_movie_l_all.avi) is confirmed by FRET measurements between native tryptophans and AEDANS dye selectively attached at a single cysteine in a Q369C mutant (Fig. 4D).

To further verify specific conformational changes predicted by the MD simulations, we have designed a spectroscopic experiment based on the following observation. As predicted by MD simulations and illustrated in Fig. 4, conformational reorganization of the protein upon protonation results in an increase in the distance between Q369 in the C-terminal of TH9 and W206 in the N-terminal of TH1 (see also Supplemental Information, SI_movie_4_W206_Q369.avi). Based on this prediction, we designed a spectroscopic experiment sensitive to changes on this distance scale by replacing Q369 with a cysteine and labeling it with bimane dye. Fluorescence of bimane has been demonstrated to be strongly

NIH-PA Author Manuscript

NIH-PA Author Manuscript

NIH-PA Author Manuscript

quenched by tryptophan in a short-distance range (less than 10 A) [31]. This is different from the relatively long-range FRET measurements described above, which are not sensitive to distance changes in this range (the Förster radius for Trp-AEDANS donor-acceptor pair is on the order of 25–30 Å). Indeed, our fluorescence lifetime measurements of bimane-labeled T-domain at pH 8 show highly quenched kinetics with a pronounced sub-nanosecond component (Fig. 4C, black curve). This quenching is relieved at pH 5.5 (red), consistent with the expectation from MD (Fig. 4A, red arrow). At intermediate pH values the kinetics can be represented by the mixture of quenched and unquenched fluorescence decays. Once the conformational change revealed by MD is validated by experiments, the MD TI procedure is used to calculate the free energy of protonation of His residues.

Thermodynamic integration and continuum electrostatics analysis of histidine protonation

We have utilized an MD-based Thermodynamic Integration (TI) approach to determine the thermodynamic consequences of protonation of individual histidines [32]. The values of free energy of protonation ΔG, calculated for all histidines in the context of the native folded state, range from somewhat favorable (e.g., for H223) to highly unfavorable (Fig. 5A). Protonation of H257 has the highest free energy penalty, and hence the most destabilizing effect on the native structure, which is consistent with our mutagenesis results[22] The free energy of protonation of H257 increases even more when calculation is repeated assuming that the neighboring H223 is already protonated (this is a reasonable assumption given the negative value of ΔG for H223).

In order to examine how the environments of individual histidine residues change during formation of the membrane-competent state, we have also calculated pKa values along the MD trajectory using a simpler continuum electrostatics approximation via solving a Poisson-Boltzmann (PB) equation numerically, as described in Computational Methods section and [26; 27]. In Fig. 5 we illustrate such pKa traces for three N-terminal histidine residues: H223, H251 and H257. (Note that we have recently demonstrated that the three C-terminal histidines do not affect folding in solution, but are important for the later steps of the membrane insertion/translocation pathway of the T-domain [23]. Therefore the PB calculations for H322, H323 and H372, shown in Fig. S2, will be discussed elsewhere.) PB calculations for the unprotonated W-state (light and dark blue, for 100 point average), plotted on a negative timescale for convenience of comparison, correspond well to more rigorous, yet computationally costly TI calculations. For all residues, the pKa values fluctuate substantially, yet the average values for H257 (4.7) and H251 (5.3) are much lower than that for H223 (6.3). The pKa traces, however, calculated along the conformational transition toward the membrane-competent state (dark yellow and red, for 100 point average), demonstrate a more complex behavior. First, the initial equilibration leads to an immediate increase in pKa, with an approximate value of 7, which is achieved via local rearrangements of atoms around either histidine residue. The subsequent dynamics, however, are quite different for the three residues, with H223 and H251 experiencing little change throughout the entire simulation time. The environment for H257, on the other hand, becomes more accommodating for the positive charge, which is reflected in the rise of its average pKa to the level of 9.5. This additional stabilization, starting at *ca.* 4 μsec, is derived from the hydrogen bonding with backbone oxygens of residues A254 and K227 (not shown).

Discussion

In this study we have used an integrated approach, which combines experimental and computational methods to characterize pH-dependent conformational switching between membrane-incompetent and -competent states of diphtheria toxin T-domain (Fig. 1). We have taken advantage of novel capabilities of the ANTON supercomputer to generate long

NIH-PA Author Manuscript

NIH-PA Author Manuscript

NIH-PA Author Manuscript

MD runs, which allowed us to observe conformational change triggered by protonation of six native histidines (Fig. 2). We verified our predictions using specifically designed spectroscopic experiments (Fig.4)which gave us confidence in applying thermodynamic analysis to histidine protonation (Fig. 5).

Our results reveal that the protonated W^+-state, originally thought of as a molten globulelike state, has a defined conformation, which nonetheless differs from that of the W-state. The main difference is that helical conformation of the TH2 segment is completely lost, while the long TH1 helix is split into two short fragments that fold on each other (Fig. 4). Interestingly, in order to get to this final conformation, TH1 is first almost completely unfolded. Similarly, the TH4 segment completely loses its helicity during early stages of transition, yet regains structure after 1.5 μsec of transition (Fig. 4B). As a result of this conformational change, the most hydrophobic helical hairpin, TH8–9, which upon interaction with membranes adopts a trans- bilayer conformation[20], becomes more exposed. In addition, conformational change, triggered by His protonation, leads to disruption of several salt bridges between different helices (e.g., K212 of TH1 and E327 of TH8). While the overall direct contribution of these relatively exposed salt bridges to protein stability is unlikely to be very high[33;34], their disruption frees positively charged residues to interact with negatively charged lipids, which were demonstrated to play a critical role during the next stages of refolding, on the lipid membrane interface[20] Thus, despite its folded structure, the W^+-state is poised to interact with the membrane and convert to the next insertion intermediate, the interfacially refolded insertion-competent state[20].

Thermodynamic integration results indicate diverse roles for different histidines in the pH-triggered conformational switching of the T-domain. For example, H223 is a likely candidate for early protonation, owing to the favorable negative free energy estimate for protonation in the context of the original structure (Fig. 5A). In contrast, H257 has the highest ΔG of protonation, thus exerting the largest perturbation on the native structure. (This is consistent with our recent mutagenesis study demonstrating partial unfolding of the H257R mutant, which is physiologically active and gains structure upon interaction with its ligand, the lipid bilayer[22].) The highest ΔG of protonation computed for H257 correlates well with the largest upward change of the pKa value of this residue computed along the protonated T-domain MD trajectory. Recently we demonstrated that the C-terminal histidines H322, H323 and H372 are important at later stages of the inertion pathway [23], although the positive ΔG values observed for H323 and H372 (as well as that for H251) suggest that their protonation is likely to contribute to the cooperativity of the initial refolding transition.

Remarkably, the free energy of protonation of H257 is raised even higher (from 6.9 to 10.2 kcal/mole) when easily protonatable H223 is charged (Fig. 5A). This suggests that H223 plays an interesting role in modulating the protonation of H257. At neutral pH, H223 gets protonated before other histidines but does not cause much of the protein unfolding (negative ΔG). Its positive charge, however, influences the protonation of H257 by increasing its free energy of protonation and hence shifting the pKa of H257 to even lower values. We further illustrate these findings in Figure 6, which presents the results of Poisson-Boltzmann calculation of pKa values for the two histidines of the diphtheria toxin T-domain, H223 and H257. In the W-state (upper panel) H223 exhibits a unimodal pKa distribution with a maximum at pKa 6.5 (blue histogram). This suggests that it is likely to be protonated even before endosomal encapsulation (pH range associated with the acidic environment of the endosome is shown as a grey band [35,36,37].) On the contrary, H257 has much lower average pKa of 4.7, distributed at two peaks centered at pH of 4 and 6.3 (green histogram). (This does not mean, however, that one needs to reach a very low pH to protonate H257 in the cell, because the T-domain undergoes a structural refolding coupled

NIH-PA Author Manuscript

NIH-PA Author Manuscript

NIH-PA Author Manuscript

with protonation. Note that the pKa distributions for the membrane-competent W^+-state (Fig. 6B) are well above the value of pH 5.5 (dotted line), at which the transition from W-to-W^+ is completed (Fig. 1).) The distribution for H257 is shifted even further to acidic pH when calculation is repeated assuming H223 is already protonated (red histogram). These differences are consistent with Thermodynamic Integration calculations (Fig. 4A), which suggest that protonation of the H257 in the context of the W-state is energetically very costly, especially when H223 is protonated. As a result the titration curve for H257 is completely removed from the range of neutral pH, and the probability of its protonation under these conditions is minimal. We hypothesize that this may be important physiologically, because otherwise the protonation of H257 would have caused substantial unfolding before the endosomal apartment is reached and would trigger a non-productive interaction with the membrane at an early stage of the insertion pathway. Thus, H223 can be compared to a safety device, which reduces protonation of the crucial H257 by further shifting its pKa, and holding it in a state resembling a loaded spring until the protein is poised for translocation in the endosomal compartment. Once acidification of an endosome lowers pH sufficiently for the protonation of H257 to occur, the safety latch can no longer hold and the spring is released, causing the conformational change that results in formation of the membrane-competent state, membrane insertion and translocation. We intend to test this safety latch hypothesis in future studies, using mutagenesis and NMR measurements of protonation of individual histidines of the T-domain.

Perspectives

MD computer simulation is a technique that can, in principle, provide a detailed, “atom-by-atom” picture of the structural reorganization of a molecule during a relatively fast relaxation process. In recent years MD methodology has been significantly refined and is becoming a widely used technique for modeling a variety of structural and dynamic properties of proteins (such as structure refinements, NMR relaxation and free energy computations). Yet its main limitation has been a relatively short timescale – typically, within tens of nanoseconds – which is certainly insufficient to analyze processes such as structural reorganization and folding/unfolding of proteins. This limitation, due to a shortage of computational power, is quickly becoming less severe, especially with the introduction of massively parallel special purpose super-computers, such as the ANTON system of Shaw Corp. [13; 14] used in this study. Here, we present simulations of the diphtheria toxin T-domain in explicit atomistic aqueous solution of a cumulative length of 8 μsee, a timescale sufficient to directly observe the conformational reconfiguration that the T-domain undergoes upon protonation of histidine residues. Various structural predictions of the simulation are verified experimentally, and thermodynamic predictions made using two alternative approaches (TI and PB calculations) are consistent with earlier mutagenesis studies.

Our results on the variation of the free energy of protonation for different histidines of the T-domain (Fig. 5A), as well as changes of the pKa of H257 along the W-to-W^+ transition (Fig. 5D), clearly illustrate that a large variation in pKa values (over 4 pH units) can be achieved in a relatively compact state and do not require substantial unfolding. This potentially enables both subtle and large-scale conformational switching by changes in pH, similar to that occurring in proteins involved in viral fusion [8; 9], assembly of multimeric proteins [38] and possibly also in intrinsically disordered (ID) proteins. The analysis of amino acid compositions of ID and folded proteins indicates that folding is promoted by higher hydrophobicity and lower mean charge Thus, protonation of histidines is expected to favor unfolding propensity, as it would introduce a charge and lower the hydrophobicity. The possibility that histidine protonation may play a role in regulation of the folding transition in ID proteins is also supported by the observation that when placed on Vihinen's flexibility

NIH-PA Author Manuscript

NIH-PA Author Manuscript

NIH-PA Author Manuscript

scale [40] with other residues, histidines occupy a borderline between residues more frequently found in folded and unfolded protein segments [39]. We expect that the integrated approach developed in this study, which relies on extended MD simulations combined with experimental verification, not only unveils the role of histidine protonation in conformational switching on later stages of the T-domain membrane-insertion pathway but will also be instrumental in the broader task of deciphering its role in regulating folding transitions in other proteins.

MATERIALS AND METHODS

Experimental methods are described in Supplemental Experimental Methods

MD simulations setup and analysis—The structural model of the T-domain (residues 201–380) was obtained from a high resolution structure of the entire toxin [Protein data bank ID code 1F0L [41]]. Hydrogen atoms and a rectangular box of water solvent molecules have been added to the protein model using AMBER 9 tLeap utility. The simulation box contained 4587 TIP3P[42] water molecules and had initial dimensions of 59 × 59 × 63 Å. The following two molecular mechanics models of the T-domain were constructed: (*a*) a model of the T-domain with histidine residues in unprotonated epsilon tautomeric form (the equivalent of membrane-incompetent W-state, populated at neutral pH) and (*b*) a model in with all six histidine residues are in the protonated form (the equivalent of membrane-competent W^+-state, populated at mildly acidic pH as illustrated in Fig. 1). Other titratable residues were kept in their standard protonation states in both models. Sodium ions were added to neutralize the charge of the system. AMBER ff99SB force field parameters were used in all simulations [43]. Periodic boundary conditions were applied and Particle Mesh Ewald (PME) method [44] with cutoff radius of 8 Å was used to compute electrostatic interactions. Energy minimization of the systems performed by steepest descent and conjugate gradient methods were followed by a 20 ns and 16 ns equilibration MD runs for the neutral pH and acidic pH models, respectively. Equilibration MD simulations were executed using the AMBER 9 PMEMD [45] program with all covalent bonds involving hydrogen atoms constrained with SHAKE [46] and a simulation time step of 2 fs. Pressure was kept at 1 atm using Berendsen barostat [47] and temperature was kept at 300 K using the Langevin thermostat [48] with a collision frequency of 2 ps^{-1}. The equilibrated structures were used as initial configurations for production of MD simulations on ANTON supercomputer [13; 14]. The parameters of production MD simulations were the same as for the equilibration run, except that the Gaussian Split Ewalds method [49] with grid size of 64 × 64 × 64 and cutoff radius 11.56 Å was used to compute electrostatic interaction. Berendsen thermostat was used to keep the temperature of the systems at 310 K with time constant of 1.2 ps. Atom coordinates were saved every 60 ps. MD simulations were carried out for 2060 ns and 6723 ns for the neutral- and the low-pH T domain models, respectively. Trajectory post-processing was performed with VMD 1.8.7 [50] and the ptraj program available in AmberTools 1.4 suite [51]. Secondary structure identification was carried out using the DSSP program [52]. Molecular figures were generated with VMD 1.8.7.

Thermodynamic Integration calculations of ΔG values of histidine protonation —Thermodynamic Integration(TI) calculations for the protonation of individual histidine residues in the T-domain in the W-state were performed using a molecular mechanics model similar to that described in Molecular Dynamics section. The computational model contained the same residues 201–380 as the T domain solvated in a periodical box with 4587 TIP3P water molecules. The AG values were computed from free energy differences of quasi-chemical transformations of histidine residues from unprotonated (δ) state to the protonated state in water $\Delta G^{water}_{unprot \rightarrow prot}$ and in the solvated protein fragment. Free energies of quasi-chemical transformation of histidine residues from the unprotonated to the protonated

NIH-PA Author Manuscript

NIH-PA Author Manuscript

NIH-PA Author Manuscript

form in water $\Delta G^{water}_{unprot \to prot}$ and in protein $\Delta G^{protein}_{unprot \to prot}$ computed from $\langle H_{prot} - H_{unprot} \rangle_\lambda$ averages over MD trajectories executed with intermediate state Hamiltonian $H_\lambda = \lambda * H_{\mathrm{unprot}} + (1-\lambda) * H_{\mathrm{prot}}$ at 3 λ values (0.11271, 0.5, 0.88729) and Gaussian quadrature formula. The length of the MD runs for each λ value was between 14 and 21 ns. All MD simulations with H_λ Hamiltonians have been started from geometry obtained after initial energy minimization of water-solvated protein fragment obtained from crystallographic structure followed by 10 ps equilibration MD run.

Continuum electrostatic (Poisson-Boltzmann) calculations—Continuum electrostatic calculations were based on finite difference solutions of the Poisson-Boltzmann equation provided by DELPHI program [24]. In this approach proteins were treated as a body of low dielectric (ε = 4) surrounded by a solvent modeled by a continuum of high dielectric constant (ε = 80). The protein and high dielectric boundary conditions were mapped in a cubic grid 121 × 121 × 121. The protein atoms van der Waals radii and charge parameters were set to PARSE radii[34] and to AMBER 94 [53] charge parameters, respectively. The radius of water molecules was set at 1.4 Å and the ionic strength was set at 0.15 M. Intrinsic pK_a values were calculated for only histidine residues and the N-terminus followed by calculation of the apparent pK_a values by Metropolis Monte-Carlo sampling [54] as implemented in HARLEM program [26;27]. The number of MC steps was 10^6, which was determined to provide converged average values. These calculations were repeated every 4 ps and 600 ps over the equilibration and production MD trajectories, respectively.

Supplementary Material

Refer to Web version on PubMed Central for supplementary material.

Acknowledgments

We are grateful to Drs. R.J. Collier, A. Fenton, L. Swint-Kruse and W.C. Wimley for their helpful comments on the safety latch hypothesis and to Mr. M. A. Myers for his editorial assistance.

ABBREVIATIONS

T-domain	diphtheria toxin T-domain
MD	Molecular Dynamics
TI	thermodynamic Integration
PB	Poisson-Boltzmann
FCS	Fluorescence Correlation Spectroscopy
FRET	Förster Resonance Energy Transfer

REFERENCES

1. Ambroggio XI, Kuhlman B. Design of protein conformational switches. Curr Opin Struct Biol. 2006; 16:525–530. [PubMed: 16765587]
2. Hoch DH, Romero-Mira M, Ehrlich BE, Finkelstein A, DasGupta BR, Simpson LL. Channels formed by botulinum, tetanus, and diphtheria toxins in planar lipid bilayers: Relevance to translocation of proteins. Proc.Natl.Acad.Sci. USA. 1985; 82:1692–1696. [PubMed: 3856850]
3. Senzel L, Huynh PD, Jakes KS, Collier RJ, Finkelstein A. The diphtheria toxin channel-forming T domain translocates its own NH_2-terminal region across planar bilayers. J.Gen.Physiol. 1998; 112:317–324. [PubMed: 9725891]

NIH-PA Author Manuscript

NIH-PA Author Manuscript

NIH-PA Author Manuscript

4. Arnon SS, Schechter R, Inglesby TV, Henderson DA, Bartlett JG, Ascher MS, Eitzen E, Fine AD, Hauer J, Layton M, Lillibridge S, Osterholm MT, O'Toole T, Parker G, Perl TM, Russell PK, Swerdlow DL, Tonat K. Botulinum toxin as a biological weapon: Medical and public health management. JAMA. 2001; 285:1059–1070. [PubMed: 11209178]
5. Neale EA. Moving across membranes. Nature Struct.Biol. 2003; 10:2–3. [PubMed: 12490883]
6. Koriazova LK, Montal M. Translocation of botulinum neurotoxin light chain protease through the heavy chain channel. Nature Struct.Biol. 2003; 10:13–18. [PubMed: 12459720]
7. Collier RJ, Young JA. Anthrax toxin. Aram Rev CellDev Biol. 2003; 19:45–70.
8. Kampmann T, Mueller DS, Mark AE, Young PR, Kobe B. The Role of histidine residues in low-pH-mediated viral membrane fysion. Structure. 2006; 14:1481–1487. [PubMed: 17027497]
9. Qin ZL, Zheng Y, Kielian M. Role of conserved histidine residues in the low-pH dependence of the Semliki Forest virus fusion protein. J Virol. 2009; 83:4670–4677. [PubMed: 19244325]
10. Hsu YT, Wolter KG, Youle RJ. Cytosol-to-membrane redistribution of Bax and Bcl-X(L) during apoptosis. Proc Natl Acad Sci USA. 1997; 94:3668–3672. [PubMed: 9108035]
11. Antignani A, Youle RJ. How do Bax and Bak lead to permeabilization of the outer mitochondrial membrane? Curr Opin Cell Biol. 2006; 18:685–689. [PubMed: 17046225]
12. Youle RJ, Strasser A. The BCL-2 protein family: opposing activities that mediate cell death. Nat Rev Mol Cell Biol. 2008; 9:47–59. [PubMed: 18097445]
13. Shaw, DE.; Bowers, KJ.; Chow, E.; Eastwood, MP.; Ierardi, DJ.; Klepeis, JL.; Kuskin, JS.; Larson, RH.; Lindorff-Larsen, K.; Maragakis, P.; Moraes, MA.; Dror, RO.; Piana, S.; Shan, Y.; Towles, B.; Salmon, JK.; Grossman, JP.; Mackenzie, KM.; Bank, JA.; Young, C.; Deneroff, MM.; Batson, B. Proceedings of the Conference on High Performance Computing Networking, Storage and Analysis - SC '09. New York, New York, USA: ACM Press; 2009. Millisecond-scale molecular dynamics simulations on Anton; p. 1
14. Shaw DE, Chao JC, Eastwood MP, Gagliardo J, Grossman JP, Ho CR, Ierardi DJ, Kolossváry I, Klepeis JL, Layman T, McLeavey C, Deneroff MM, Moraes MA, Mueller R, Priest EC, Shan Y, Spengler J, Theobald M, Towles B, Wang SC, Dror RO, Kuskin JS, Larson RH, Salmon JK, Young C, Batson B, Bowers KJ. Anton, a special-purpose machine for molecular dynamics simulation. ACMSIGARCH Computer Architecture News. 2007; 35:1.
15. Oh KJ, Senzel L, Collier RJ, Finkelstein A. Translocation of the catalytic domain of diphtheria toxin across planar phospholipid bilayers by its own T domain. Proc.Natl.Acad.Sci. USA. 1999; 96:8467–8470. [PubMed: 10411898]
16. Bennett MJ, Eisenberg D. Refined structure of monomeric diphtheria toxin at 2.3 A resolution. Protein Sci. 1994; 3:1464–1475. [PubMed: 7833808]
17. Oh KJ, Zhan H, Cui C, Hideg K, Collier RJ, Hubbell WL. Organization of diphtheria toxin T domain in bilayers: A site-directed spin labeling study. Science. 1996; 273:810–812. [PubMed: 8670424]
18. Kachel K, Ren JH, Collier RJ, London E. Identifying transmembrane states and defining the membrane insertion boundaries of hydrophobic helices in membrane-inserted diphtheria toxin T domain. J.Biol.Chem. 1998; 273:22950–22956. [PubMed: 9722516]
19. Senzel L, Gordon M, Blaustein RO, Oh KJ, Collier RJ, Finkelstein A. Topography of diphtheria toxin's T domain in the open channel state. J.Gen.Physiol. 2000; 115:421–434. [PubMed: 10736310]
20. Kyrychenko A, Posokhov YO, Rodnin MV, Ladokhin AS. Kinetic intermediate reveals staggered pH-dependent transitions along the membrane insertion pathway of the diphtheria toxin T-domain. Biochemistry. 2009; 48:7584–7594. [PubMed: 19588969]
21. Perier A, Chassaing A, Raffestin S, Pichard S, Masella M, Menez A, Forge V, Chenal A, Gillet D. Concerted protonation of key histidines triggers membrane interaction of the diphtheria toxin T domain. J Biol Chem. 2007; 282:24239–24245. [PubMed: 17584737]
22. Rodnin MV, Kyrychenko A, Kienker P, Sharma O, Posokhov YO, Collier RJ, Finkelstein A, Ladokhin AS. Conformational switching of the diphtheria toxin T domain. J Mol Biol. 2010; 402:1–7. [PubMed: 20654627]

NIH-PA Author Manuscript

NIH-PA Author Manuscript

NIH-PA Author Manuscript

23. Rodnin MV, Kyrychenko A, Kienker P, Sharma O, Vargas-Uribe M, Collier RJ, Finkelstein A, Ladokhin AS. Replacement of C-terminal histidines uncouples membrane insertion and translocation in diphtheria toxin T-domain. Biophys J. 2011; 101:L41–L43. [PubMed: 22098755]
24. Nicholls A, Honig B. A rapid finite difference algorithm, utilizing successive over-relaxation to solve the Poisson-Boltzmann equation. Journal of Computational Chemistry. 1991; 12:435–445.
25. Yang AS, Gunner MR, Sampogna R, Sharp K, Honig B. On the calculation of pKas in proteins. Proteins. 1993; 15:252–265. [PubMed: 7681210]
26. Kurnikov IV, Ratner MA, Pacheco AA. Redox equilibria in hydroxylamine oxidoreductase. Electrostatic control of electron redistribution in multielectron oxidative processes. Biochemistry. 2005; 44:1856–1863. [PubMed: 15697211]
27. Kurnikov IV. HARLEM, Molecular Modeling Package. 2002
28. Palchevskyy SS, Posokhov YO, Olivier B, Popot JL, Pucci B, Ladokhin AS. Chaperoning of Insertion of Membrane Proteins into Lipid Bilayers by Hemifluorinated Surfactants: Application to Diphtheria Toxin. Biochemistry. 2006; 45:2629–2635. [PubMed: 16489756]
29. Rodnin MV, Posokhov YO, Contino-Pepin C, Brettmann J, Kyrychenko A, Palchevskyy SS, Pucci B, Ladokhin AS. Interactions of fluorinated surfactants with diphtheria toxin T-domain: testing new media for studies of membrane proteins. Biophys J. 2008; 94:4348–4357. [PubMed: 18310255]
30. Ladokhin AS, White SH. Folding of amphipathic a-helices on membranes: Energetics of helix formation by melittin. J.Mol.Biol. 1999; 285:1363–1369. [PubMed: 9917380]
31. Mansoor SE, Mchaourab HS, Farrens DL. Mapping proximity within proteins using fluorescence spectroscopy. A study of T4 lysozyme showing that tryptophan residues quench bimane fluorescence. Biochemistry. 2002; 41:2475–2484. [PubMed: 11851393]
32. Mamonova T, Yonkunas MJ, Kurnikova MG. Energetics of the cleft closing transition and the role of electrostatic interactions in conformational rearrangements of the glutamate receptor ligand binding domain. Biochemistry. 2008; 47:11077–11085. [PubMed: 18823129]
33. Nicholls A, Sharp KA, Honig B. Protein folding and association: Insights from the interfacial and thermodynamic properties of hydrocarbons. Proteins. 1991; 11:281–296. [PubMed: 1758883]
34. Sitkoff D, Sharp KA, Honig B. Accurate calculation of hydration free energies using macroscopic solvent models. J.Phys.Chem. 1994; 98:1978–1988.
35. Murphy RF, Powers S, Cantor CR. Endosome pH measured in single cells by dual fluorescence flow cytometry: rapid acidification of insulin to pH 6. The Journal of Cell Biology. 1984; 98:1757–1762. [PubMed: 6144684]
36. Yamashiro DJ, Maxfield FR. Kinetics of endosome acidification in mutant and wild-type Chinese hamster ovary cells. The Journal of Cell Biology. 1987; 105:2713–2721. [PubMed: 2447097]
37. Huotari J, Helenius A. Endosome maturation. EMBO J. 2011; 30:3481–3500. [PubMed: 21878991]
38. Dang LT, Purvis AR, Huang RH, Westfield LA, Sadler JE. Phylogenetic and functional analysis of histidine residues essential for pH-dependent multimerization of von Willebrand factor. J Biol Chem. 2011; 286:25763–25769. [PubMed: 21592973]
39. Uversky VN, Dunker AK. Understanding protein non-folding. Biochim Biophys Acta. 2010; 1804:1231–1264. [PubMed: 20117254]
40. Vihinen M, Torkkila E, Riikonen P. Accuracy of protein flexibility predictions. Proteins. 1994; 19:141–149. [PubMed: 8090708]
41. Steere, B. Characterization of high-order oligomerization and energetics in Diptheria Toxin. Los Angeles: University of California; 2001. PhD Thesis
42. Jorgensen WL, Chandrasekhar J, Madura JD, Impey RW, Klein ML. Comparison of simple potential functions for simulating liquid water. J.Chem.Phys. 1983; 79:926–935.
43. Hornak V, Abel R, Okur A, Strockbine B, Roitberg A, Simmerling C. Comparison of multiple Amber force fields and development of improved protein backbone parameters. Proteins. 2006; 65:712–725. [PubMed: 16981200]
44. Darden T, York D, Pedersen L. Particle mesh Ewald: An Nlog(N) method for Ewald sums in large systems. The Journal of Chemical Physics. 1993; 98:10089–10092.

NIH-PA Author Manuscript

NIH-PA Author Manuscript

NIH-PA Author Manuscript

45. Case, DA.; Darden, TA.; Cheatham, TESCL., III; Wang, J.; Duke, RE.; Luo, R.; Merz, KM.; Pearlman, DA.; Crowley, M.; Walker, RCWZ.; Wang, B.; Hayik, S.; Roitberg, A.; Seabra, G.; Wong, KF.; Paesani, F.; Wu, X.; Brozell, S.; Tsui, V.; Gohlke, H.; Yang, L.; Tan, C.; Mongan, J.; Hornak, V.; Cui, G.; Beroza, P.; Mathews, DH.; Schafmeister, C.; Ross, WS.; Kollman, PA. AMBER 9. San Francisco: University of California; 2006.

46. Ryckaert J-P, Ciccotti G, Berendsen HJC. Numerical integration of the Cartesian equations of motion of a system with constraints: Molecular dynamics of *n*-alkanes. J.Comput.Phys. 1977; 23:327–341.

47. Berendsen HJC, Postma JPM, van Gunsteren WF, DiNola A, Haak JR. Molecular dynamics with coupling to an external bath. J.Chem.Phys. 1984; 81:3684–3690.

48. Pastor RW, Brooks BR, Szabo A. An analysis of the accuracy of Langevin and molecular dynamics algorithms. Molecular Physics. 1988; 65:1409–1419.

49. Shan Y, Klepeis JL, Eastwood MP, Dror RO, Shaw DE. Gaussian split Ewald: A fast Ewald mesh method for molecular simulation. The Journal of Chemical Physics. 2005; 122:054101.

50. Humphrey W, Dalke A, Schulten K. VMD: visual molecular dynamics. Journal of molecular graphics. 1996; 14:33–38. [PubMed: 8744570]

51. Case, DA.; Darden, TA.; Cheatham, TE., III; Simmerling, C.; Wang, J.; Duke, RE.; Luo, R.; Walker, RC.; Zhang, W.; Merz, KM.; Roberts, BP.; Hayik, S.; Roitberg, A.; Seabra, G.; Kolossvary, I.; Wong, KF.; Paesani, F.; Vanicek, J.; Liu, J.; Wu, X.; Brozell, SR.; Steinbrecher, T.; Gohlke, H.; Cai, Q.; Ye, X.; Wang, J.; Hsieh, M-J.; Hornak, V.; Cui, G.; Roe, DR.; Mathews, DH.; Seetin, MG.; Sagui, C.; Babin, V.; Luchko, T.; Gusarov, S.; Kovalenko, A.; Kollman, PA. AMBER 11. San Francisco: University of California; 2010. University of California, San Francisco

52. Kabsch W, Sander C. Dictionary of protein secondary structure: Pattern recognition of hydrogen-bonded geometrical feature. Biopolymers. 1983; 22:2577–2637. [PubMed: 6667333]

53. Cornell WD, Cieplak P, Bayly CI, Gould IR, Merz KM, Ferguson DM, Spellmeyer DC, Fox T, Caldwell JW, Kollman PA. A 2nd Generation Force-Field for the Simulation of Proteins, Nucleic-Acids, and Organic-Molecules. Journal of the American Chemical Society. 1995; 117:5179–5197.

54. Bashford D, Karplus M. Multiple-site titration curves of proteins: an analysis of exact and approximate methods for their calculation. The Journal of Physical Chemistry. 1991; 95:9556–9561.

NIH-PA Author Manuscript

NIH-PA Author Manuscript

NIH-PA Author Manuscript

- Conformational switching is investigated by computational and experimental methods
- Microsecond MD simulations reveal conformational change upon histidine protonation
- Thermodynamic integration is used to calculate free energy of histidine protonation
- Protonation of H257 ensures conformational changes
- Protonation of H223 protects from premature protonation of H257

NIH-PA Author Manuscript
NIH-PA Author Manuscript
NIH-PA Author Manuscript

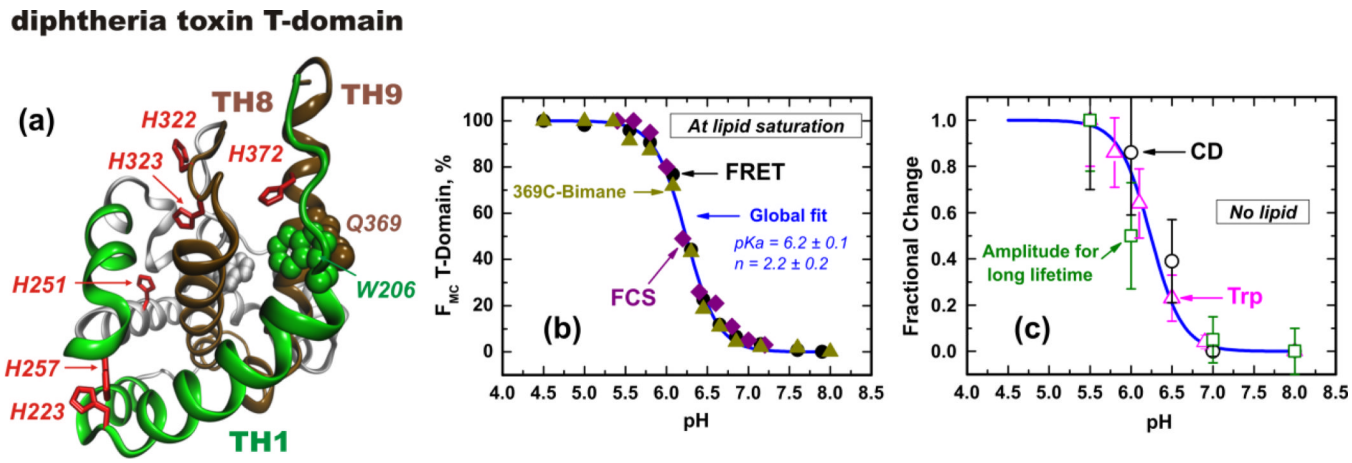

Figure 1.

(A) Crystallographic structure of the diphtheria toxin T-domain[16] is represented as a backbone ribbon with the hydrophobic membrane insertion hairpin TH8–9 highlighted in brown. Protonation of histidine residues (shown as red sticks) is implicated in modulating pH-dependent refolding of the T-domain, which is studied here by various computational methods (see Fig. 5). Extended MD simulations indicate unfolding/refolding of the long N-terminal helix TH1 and helix TH2 (shown in green) is an important step in the formation of membrane-competent state of the T-domain (see Fig. 2 and Supplemental Information movies, SI_movie_l_all.avi, SI_movie_THl_TH2.avi). Changes in proximity of residues W206 and Q369 (shown as space filling structures) are used to verify the predictions of the MD simulations using methods of fluorescence spectroscopy (see Fig. 4). Grey space filling structure corresponds to W281. **(B and C) pH-Dependent conversion of T-domain from soluble W-state into membrane-competent W^+-state**. (B) Identification of W-to-W^+ transition through membrane binding at lipid saturation. FCS-based mobility measurements (diamonds) and measurements of FRET between donor-labeled T-domain and acceptor-labeled vesicles (circles) were performed as described in with raw data presented in SI Fig. SI A. Triangles represent increase in fluorescence of environment-sensitive probe bimane attached to a single cysteine in position 369. Solid line represents a fit of combined data with Eq. 4 of the Supplemental Experimental Methods. (C) Identification of W-to-W^+ transition through spectroscopic measurements in the absence of lipid. Relative changes in Trp intensity (triangles), ellipticity at 222 nm (circles) are the averages of triplicate measurements. Squares represent relative changes in the amplitude of the unquenched lifetime component of fluorescence decay component of bimane dye attached to residue 369 (more on quenching mechanism in text and in Fig. 4). The error bars for bimane amplitude represent results of the support-plane analysis that accounts for the cross-correlation of the fluorescence decay parameters. All data are presented as fractional changes in the corresponding signals between values measured at pH 8.0 and 5.5 (representative raw data are shown in Fig. 4C and SI Figs. SIB and SIC) and overlaid with the fit to binding data from panel B (solid line) for visual reference.

NIH-PA Author Manuscript

NIH-PA Author Manuscript

NIH-PA Author Manuscript

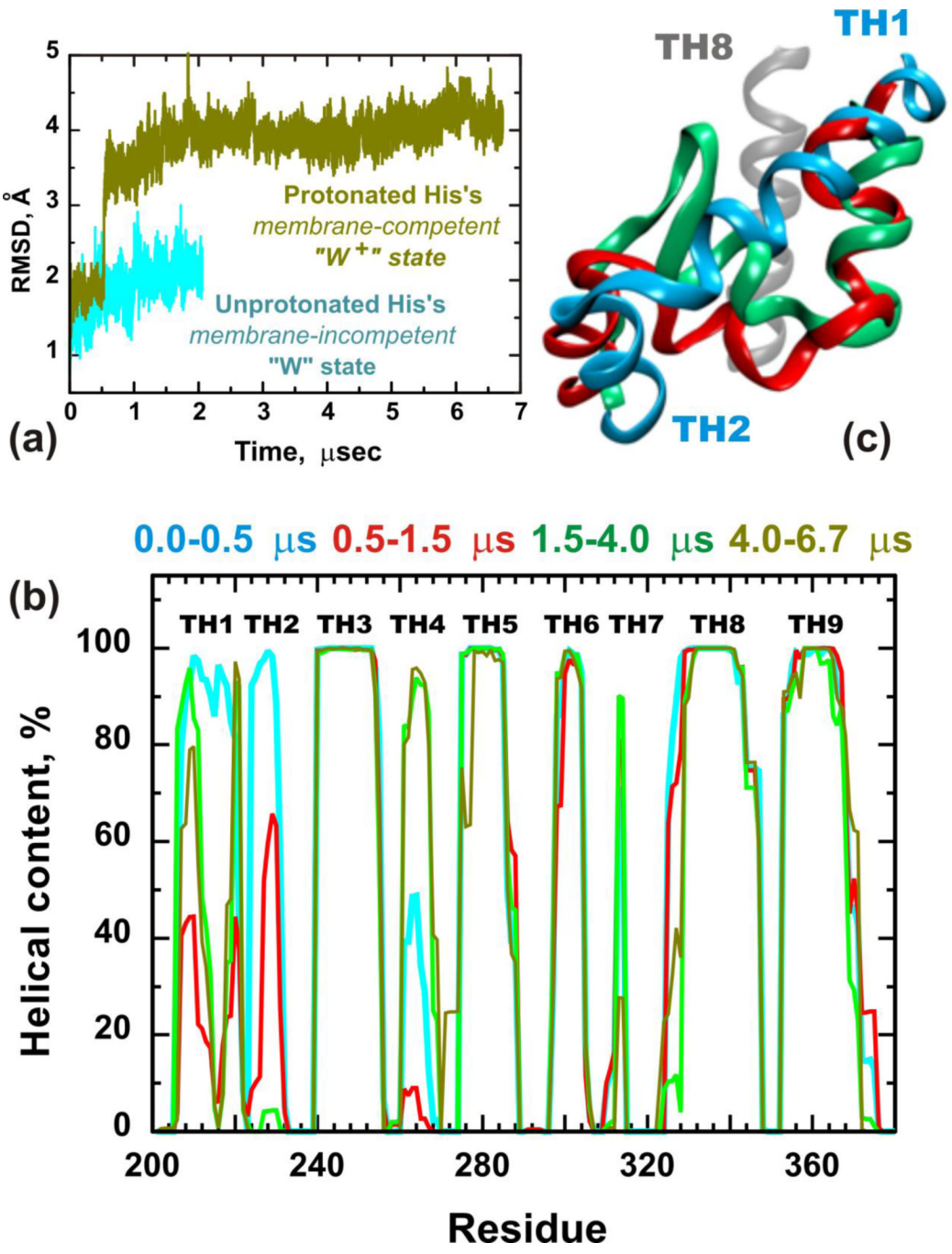

Figure 2. Conformational changes in T-domain triggered by histidine protonation established by MD simulations

(A) Comparison of RMSD traces obtained from MD runs with unprotonated (blue trace) and protonated histidines (yellow trace). MD-generated structures were rotated and translated to minimize the RMSD values relative to crystallographic coordinates of Ca atoms in helices TH1 to TH9. The conformational transition apparent from the abrupt change in the latter trace at ~0.5 μs affects the secondary (B) and tertiary structure (C) of the T-domain in the W^+-state. (B) Changes in helical content obtained by averaging the probability of helical conformation during four different stages of the conformational transition triggered by histidine protonation. Colored lines represent (i) initial membrane-incompetent W-state

NIH-PA Author Manuscript

NIH-PA Author Manuscript

NIH-PA Author Manuscript

(blue, 0–0.5 μs); (ii) main conformational transition (red, 0.5–1.5 μs); (iii) subsequent refolding (green, 1.5–4.0 μs) and final conformation of membrane-competent W^+-state (yellow, 4.0–6.7)μs). These data indicate the loss of helical structure corresponding to crystallographic helices TH2 and TH7 as well as refolding of a long helix TH1 into two short helical segments. (C) MD snapshots illustrating the changes in fold of the TH1–2 helical region. The original structure formed by two well-defined helices (198.42 ns snapshot, blue) is lost during conformational change caused by histidine protonation (800.58 ns, red) and is transformed into two short helical regions folded against each other and a substantial unfolded segment (2878.92 ns, green). This refolding also substantially increases the distance between H223 and H257 (SI_movie_3_H223_H257.avi). As a result, the most hydrophobic helix TH8 (grey) becomes more accessible for subsequent interaction with the lipid bilayer.

NIH-PA Author Manuscript

NIH-PA Author Manuscript

NIH-PA Author Manuscript

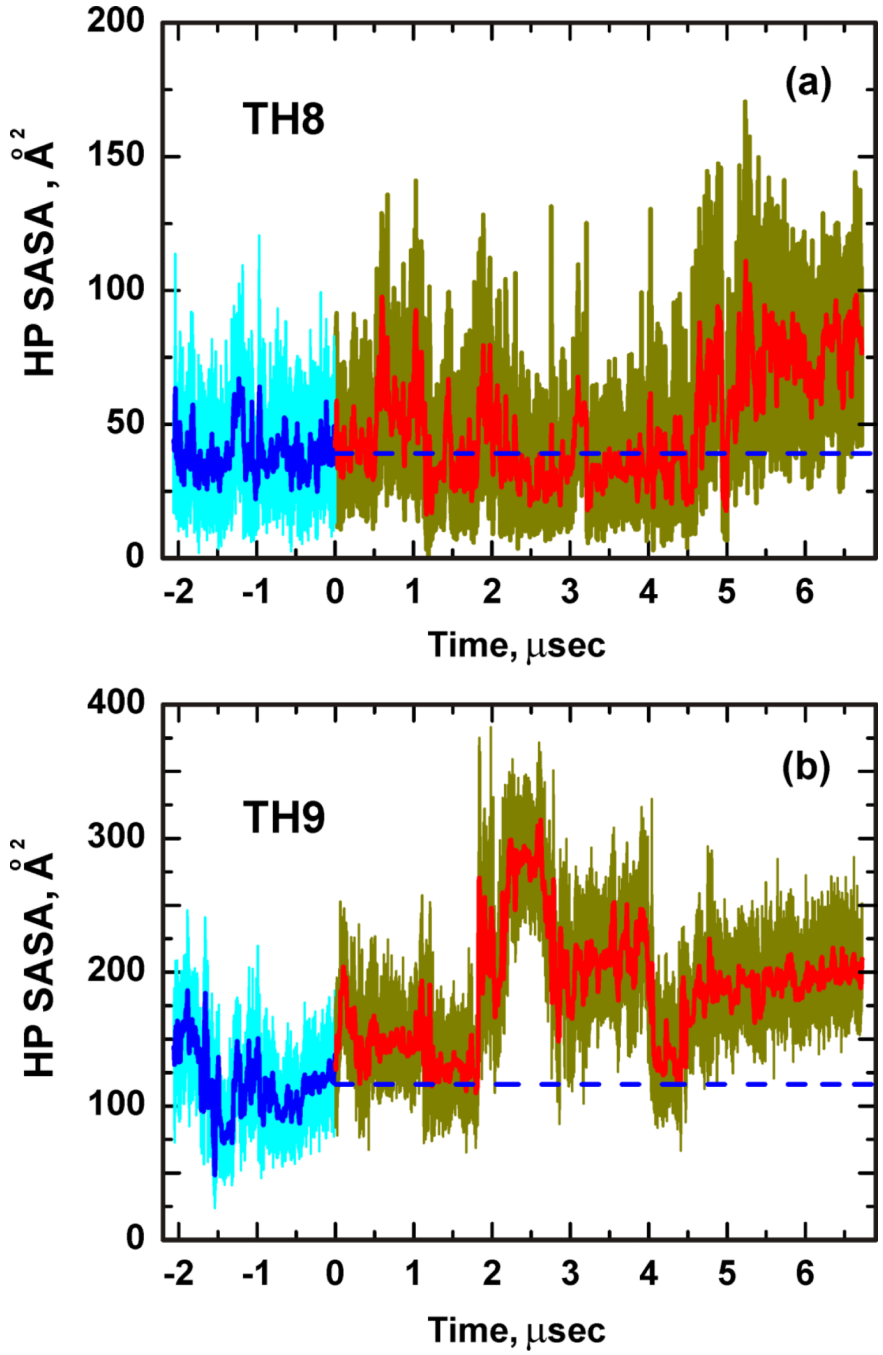

Figure 3. Changes in solvent accessible surface area (SASA) of hydrophobic side chains in helices TH8 (A) and TH9 (B)

The light blue and yellow traces correspond to the MD simulations with neutral and protonated histidines respectively. The dark blue and red lines represent running averages over a 60 ns window. Blue dotted lines are drawn for visual representation of the average SASA values in the W-state for TH8 (SASA=39), and TH9 (SASA=116).

NIH-PA Author Manuscript
NIH-PA Author Manuscript
NIH-PA Author Manuscript

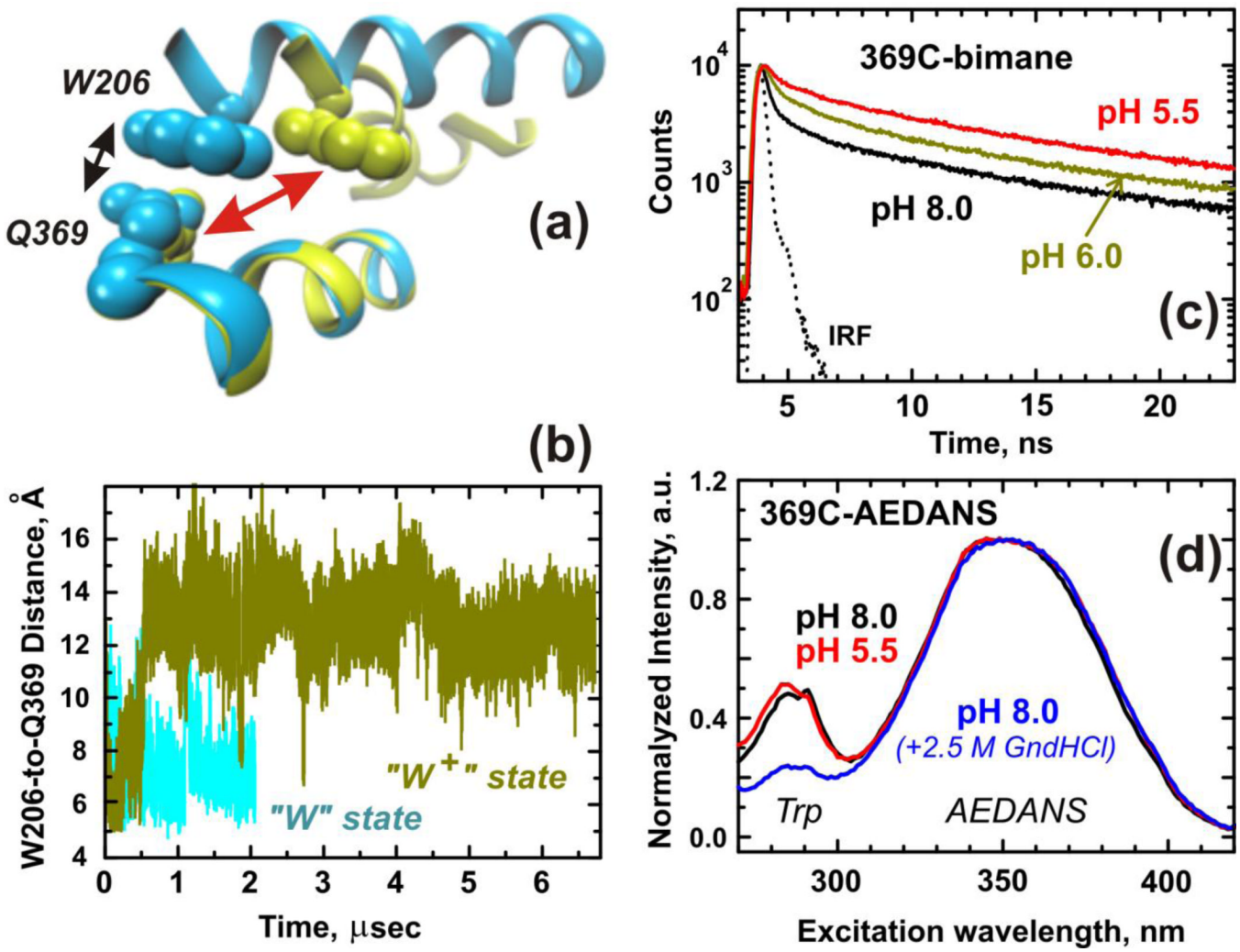

Figure 4.

Experimental validation of the MD-predicted structural changes between membrane-incompeten W-state (illustrated by 459.54 ns snapshot structure in blue) and membrane-competent W^+-state (illustrated by 4865.22 ns snapshot structure in yellow). (A) The W-to-W^+ conformational rearrangement triggered by histidine protonation and illustrated in Fig. 2 results in a change in proximity of residues Q369 (C-terminal helix TH9) and W206 (N-terminal helix TH1), which can be verified by two specifically designed fluorescence experiments. (B) Distance between alpha-carbons of W206 and Q369 from MD simulation of nonprotonated (blue) and protonated T-domain (yellow). (C) Validation of proximity changes in panel A by short-range aromatic quenching[31] of bimane probe attached to single cysteine mutant at position 369: fluorescence decay following the pulsed excitation is strongly quenched in W-state (pH 8, black line), but not in W^+-state (pH 5.5, red line). (D) Long-range FRET measurements between two donors, W206 and W281, and AEDANS acceptor probe attached to single cysteine mutant at position 369: excitation spectra measured at 500 nm at pH 8.0 (black line) and 5.5 (red line) showed no variation in FRET level, while unfolding with guanidine HC1 (blue line) reduced FRET, as seen by the loss of donor contribution at 280–290 nm. Both spectroscopic experiments confirm MD results, suggesting local rearrangements but not a global refolding for W-to-W transition.

NIH-PA Author Manuscript
NIH-PA Author Manuscript
NIH-PA Author Manuscript

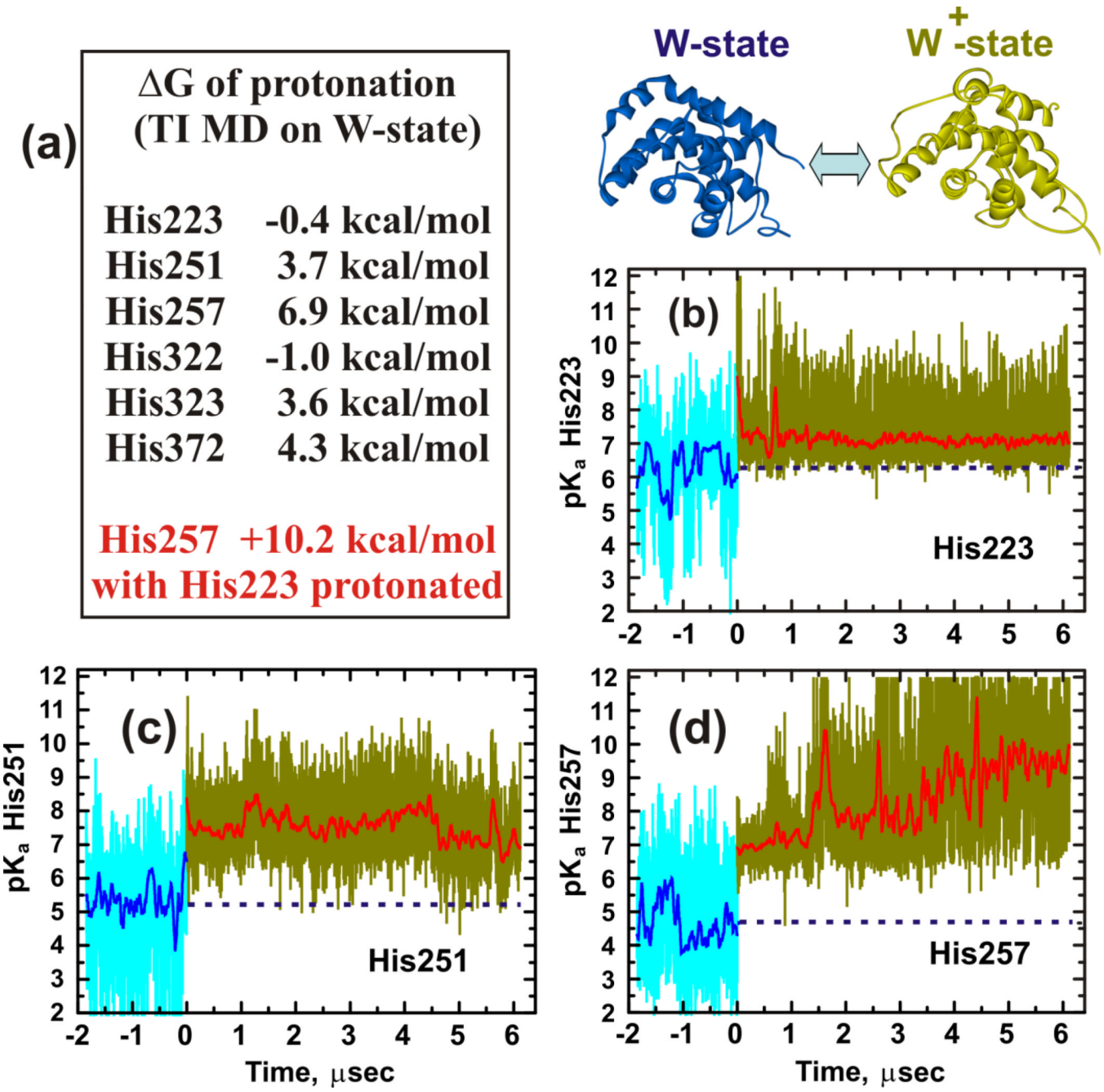

Figure 5. Thermodynamics of histidine protonation in the T-domain

(A) TI calculations of the free energy of protonation ΔG of all of the histidines (see text for details). Time traces of pKa's for residues H223 (B), H251 (C) and H257 (D) calculated using PB approach from the MD simulations. Light blue and yellow traces correspond to the calculation for MD simulations with nonprotonated and protonated histidines, respectively (Fig. 2A), while dark blue and red represent corresponding pKa traces averaged over a 60 ns-window (pKa values were calculated from MD-generated structures every 600 ps). Blue dotted lines are drawn for visual representation of the average pKa values in the W-state for H223 (average pKa=6.3), H251 (average pKa=5.3) and H257 (average pKa=4.7). As further discussed in the text, both TI and PB calculations indicate different roles for H257 (difficult

NIH-PA Author Manuscript

NIH-PA Author Manuscript

NIH-PA Author Manuscript

to protonate in the W-state; protonation provides the major driving force of refolding into the W^+-state) and H223 (easy to protonate in the W-state, prevents premature protonation of H257).

NIH-PA Author Manuscript

NIH-PA Author Manuscript

NIH-PA Author Manuscript

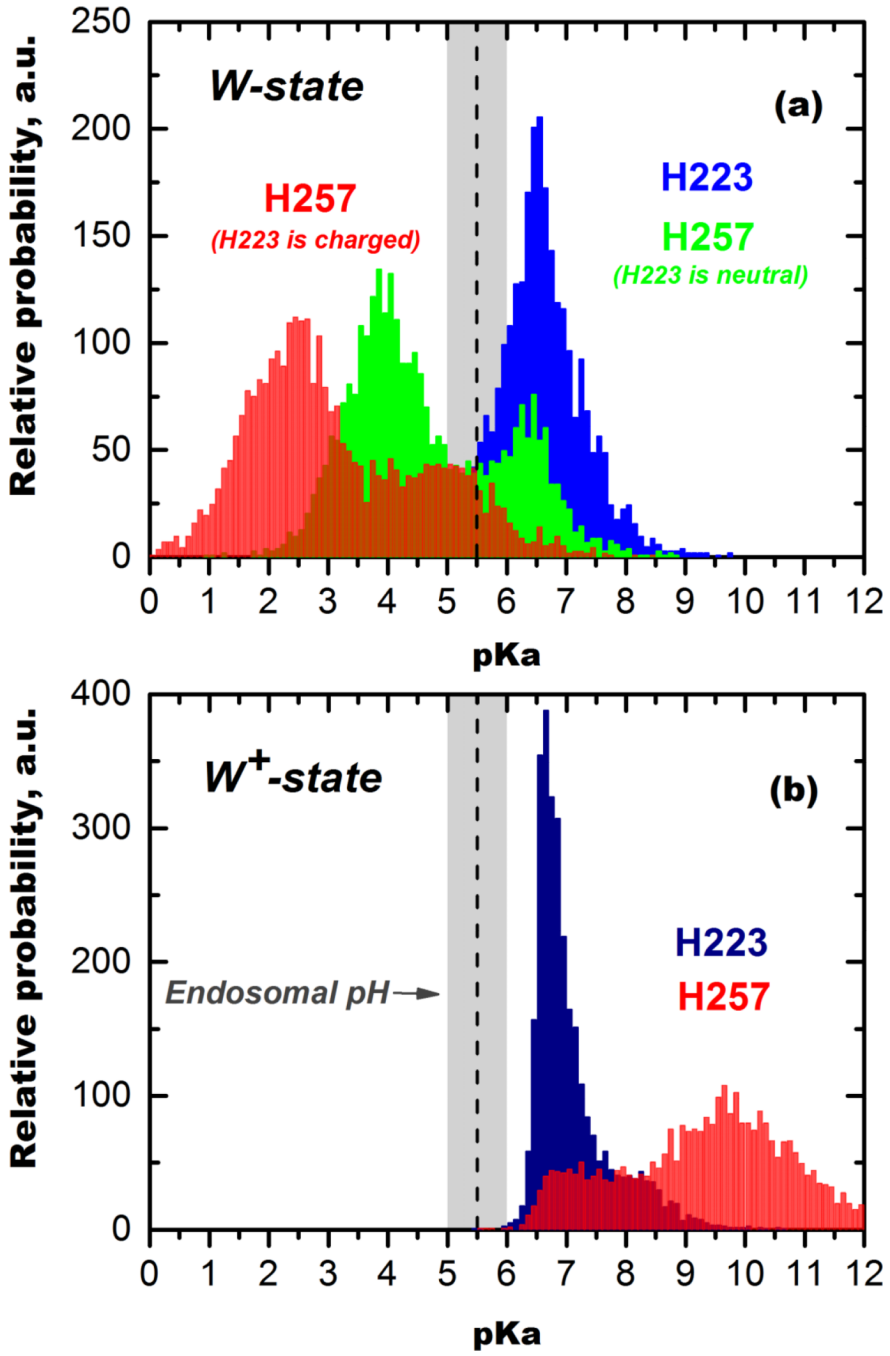

Figure 6.

pKa distributions of key histidine residues, H223 and H257, calculated in PB approximation from MD traces for (A) membrane-incompetent W-state and (B) membrane-competent W^+-state (region of 4.0–6.7 μsec in protonated MD run from Fig. 5 B, D) (see text for details).